

# Cross correlation of Lyman- $\alpha$ absorbers with gas-rich galaxies

Emma V. Ryan-Weber<sup>1\*</sup>

<sup>1</sup>*Institute of Astronomy, University of Cambridge, Madingley Rd, Cambridge CB3 0HA, UK*

Accepted 2006 January 3. Received 2005 December 20; in original form 2005 October 17

## ABSTRACT

The H I Parkes All Sky Survey (HIPASS) galaxy catalogue is cross-correlated with known low redshift, low column density ( $N_{\text{HI}} < 10^{15} \text{ cm}^{-2}$ ) Lyman- $\alpha$  absorbers from the literature. The redshift-space correlation is found to be similar in strength to HIPASS galaxy self-clustering (correlation length  $s_{0,ag} = 6 \pm 4$  and  $s_{0,gg} = 3.1 \pm 0.5 h_{100}^{-1}$  Mpc respectively). In real-space the cross-correlation is stronger than the galaxy auto-correlation (correlation length  $r_{0,ag} = 7.2 \pm 1.4$  and  $r_{0,gg} = 3.5 \pm 0.7 h_{100}^{-1}$  Mpc respectively) on scales from  $1 - 10 h_{100}^{-1}$  Mpc, ruling out the mini-halo model for the confinement Ly $\alpha$  absorbers at the 99 percent confidence level. Provided that the cause of the strong cross-correlation is purely gravitational, the ratio of correlation lengths suggest that absorbers are embedded in dark matter haloes with masses  $\log(M/M_{\odot}) = 14.2 h_{100}^{-1}$ , similar to those of galaxy groups. The flattening of the cross-correlation at separations less than  $\sim 600 h_{100}^{-1}$  kpc could correspond to the thickness of filaments in which absorbers are embedded. This work provides indirect statistical evidence for the notion that galaxy groups and large-scale filaments, particularly those that comprise gas-rich galaxies, are the dominant environments of low column density Ly $\alpha$  absorbers at  $z = 0$ .

**Key words:** intergalactic medium, quasars: absorption lines, galaxies: statistics, large-scale structure of universe

## 1 INTRODUCTION

At the present epoch less than 10 per cent of baryonic matter is located in galaxies (Cole et al. 2001; Zwaan et al. 2003). The majority of baryons therefore lie in the intergalactic medium (IGM), and knowledge of the distribution of these baryons is essential to our understanding of how matter is organised in the Universe. Lyman- $\alpha$  (Ly $\alpha$ ) absorption towards distant quasars reveals the presence of neutral hydrogen (H I) in the IGM. At low redshift, observations show that these low column density ( $N_{\text{HI}} < 10^{15} \text{ cm}^{-2}$ ) absorbers exist in a variety of environments, including large-scale filaments (e.g. Le Brun et al. 1996; Penton et al. 2002; Rosenberg et al. 2003), galaxy groups (e.g. Lanzetta et al. 1996; Bowen et al. 2002), and even voids (McLin et al. 2002) and underdense regions (Grogin & Geller 1998). A positive connection between absorbers and galaxies has been established by many studies (Morris et al. 1993; Lanzetta et al. 1995; Bowen et al. 1996; Tripp et al. 1998; Chen et al. 1998, 2001; Impey et al. 1999; Ortiz-Gil et al. 1999), however most conclude that a one-to-one correspondence between absorbers and individual galaxies does not exist. Côté et al. (2005) and Putman et al. (2006) provide compelling evidence that absorbers trace the cosmic web, finding that absorbers at large radii do not follow galactic rotation curves. Thus the absorbers appear to lie in the same overdensities as the galaxies, but not in individual galaxy haloes.

Despite the absorbers' positive association with highly biased, strongly clustered objects, i.e. galaxies and large-scale structures, low- $N_{\text{HI}}$  Ly $\alpha$  absorbers are among the weakest self-clustering objects in the low redshift Universe. The two-point correlation function in velocity separation,  $\Delta v$ , shows mild absorber clustering for  $\Delta v \lesssim 500 \text{ km s}^{-1}$  (Tripp et al. 1998; Impey et al. 1999; Dobrzycki et al. 2002; Penton et al. 2002), weaker than that of galaxy self-clustering (although, see Ulmer 1996). Hydrodynamic simulations also measure weak clustering of small gas overdensities in velocity space (Davé et al. 2003), these overdensities,  $0.5 < \log(\rho_H/\bar{\rho}_H) < 1.5$ , correspond to Ly $\alpha$  absorbers with  $13 \lesssim \log(N_{\text{HI}}/\text{cm}^{-2}) \lesssim 14$  (Davé et al. 1999). When compared with galaxies identified in the simulations, a filamentary structure emerges, where absorbers of increasing column density arise in closer proximity to galaxies.

The cross-correlation function of absorbers and galaxies can be used to measure the extent to which the two populations of objects are associated. At intermediate redshifts the strong cross-correlation between Lyman break galaxies and C IV absorbers is used to argue that these two populations are in fact the same object (Adelberger et al. 2005). The spatial co-incidence of C IV absorbers and Lyman break galaxies however can equally be interpreted as pre-enrichment from dwarf galaxies born from the collapse of  $\sim 2\sigma$  fluctuations at  $6 < z < 12$  (Madau et al. 2001; Porciani & Madau 2005). The same degeneracy has the potential to plague the interpretation of the cross-correlation of absorbers and galaxies at  $z = 0$ . How can we tell the difference between a

\* email: eryl@ast.cam.ac.uk

strong cross-correlation signal due to absorbers arising in galaxy haloes and that due to a general overdensity of matter that surrounds galaxies? This issue is related to the claim that  $10^{14} \lesssim N_{\text{HI}} \lesssim 10^{18} \text{ cm}^{-2}$  absorbers arise within the haloes of galaxies, based on the anti-correlation between impact parameter and Ly $\alpha$  absorber equivalent width (Lanzetta et al. 1995; Chen et al. 1998, 2001). Solid observational evidence (Bowen et al. 2002; Côté et al. 2005), numerical simulations (Davé et al. 1999) and analytic models (Lin et al. 2000) have now resolved this degeneracy, showing that the anti-correlation between absorber-galaxy separation and density of absorbing material is a natural consequence of the overdensity of matter that surrounds galaxies, extending well beyond galaxy haloes. Since we know that absorbers and galaxies are largely not the same object, their cross-correlation signal can be used to measure the extent to which they are associated. The cross-correlation signal can also, subject to interpretation, provide an indirect method to measure the bias of the absorbers, i.e. the relationship between HI column density and underlying dark matter density.

In the Press–Schechter (PS, Press & Schechter 1974) formalism, the ratio of the bias of two populations of objects is equal to the ratio of the cross- to auto-correlation function (e.g. Mo & White 1996, 2002).<sup>1</sup> Therefore, by (i) knowing the characteristic total (dark plus baryonic) halo mass of a galaxy population, (ii) measuring the galaxy auto-correlation function, and (iii) measuring the absorber-galaxy cross-correlation function, the mass of the haloes in which the absorbers are embedded can be inferred. This method has been successfully used by Bouché et al. (2004). They cross-correlated Mg II absorbers with Luminous Red Galaxies (LRGs) to show that the Mg II absorbers are embedded in haloes with masses  $\sim 2 - 8 \times 10^{11} M_{\odot}$ , consistent with the expectation that  $\sim 40$  per cent of Mg II absorbers arise in Damped Ly $\alpha$  (DLA) systems (Rao et al. 2006), and that DLAs are expected to have total halo masses of that order. DLAs are gravitationally collapsed objects and at low redshift are consistent with the local galaxy population weighted by HI cross section (Zwaan et al. 2005). Lower column density absorbers are not collapsed and may not follow the same bias trends. At intermediate redshifts the distribution of Ly $\alpha$  absorbers reveal structures on scales up to  $17 h_{100}^{-1}$  Mpc (Liske et al. 2000), at these redshifts the bias and clustering properties of Ly $\alpha$  absorbers are well modelled (Cen et al. 1998; McDonald et al. 2002). However the physics of the IGM increases in complexity towards  $z = 0$ . As noted by Davé et al. (2003) the correlation function of gas overdensity no longer follows the correlation function of HI optical depth at  $z = 0$ , showing that the bias is not as predictable as at higher redshifts. Some models however place absorbers in individual mini-haloes, which do have a well defined bias.

Mini-halo models predict that absorbers arise in gravitationally confined gas within dark matter mini-haloes (Ikeuchi 1986; Rees 1986; Mo & Morris 1994). Since mini-haloes are less massive than galaxy haloes, the absorber-galaxy cross-correlation is expected to be weaker than the galaxy auto-correlation. The mini-halo model is not an ideal description of Ly $\alpha$  absorbers. Too many haloes per unit redshift are required to account for the observed density of absorption lines, since the mini-haloes have small spatial cross sections.

<sup>1</sup> In this paper the function that compares the same population of objects is referred to as the auto-correlation, and the function that compares two populations is referred to as the cross-correlation.

The absorber-galaxy cross-correlation function is instrumental in establishing whether absorbers are associated with individual mini-haloes, galaxies or large-scale structure. Although other statistics have been used by other authors, such as nearest neighbour and galaxy density distributions, the properties of the cross-correlation function can be related to the underlying dark matter density. The cross-correlation is also a clean statistic as it does not rely on assumptions about correlated pairs. Morris et al. (1993) is the only  $z = 0$  absorber-galaxy cross-correlation function published to-date that includes a full three-dimensional calculation. They used 17 absorbers along the 3C 273 line-of-sight and found that the absorber-galaxy cross-correlation is weaker than the galaxy auto-correlation on scales from  $1 - 10 h_{80}^{-1}$  Mpc. Mo & Morris (1994) explain this finding with a combination of 20 – 30 per cent of absorbers arising in galaxies and the remainder arising in mini-haloes.

In this paper the cross-correlation function is calculated using 129 absorbers along 27 lines-of-sight from the literature and 5,317 galaxies from a blind 21-cm emission-line survey. The galaxy and absorber data are described in Section 2. The details of the cross-correlation and halo-mass calculation methods are described in Section 3. The subsequent results are outlined in Section 4, including the redshift- and real-space correlation functions. The nature of the Ly $\alpha$  absorber correlation signal and its relationship to galaxies, groups of galaxies and large-scale filaments is discussed in Section 5, with a final summary given in Section 6. To compare with correlation functions in the literature  $H_0 = 100 \text{ km s}^{-1} \text{ Mpc}^{-1}$  is used throughout.

## 2 DATA AND RANDOM SAMPLES

### 2.1 HIPASS Galaxies

The HI Parkes All Sky Survey (HIPASS) is a blind survey for extragalactic 21-cm emission, thus it provides a census of gas-rich galaxies at  $z = 0$ . Extragalactic sources in HIPASS have been catalogued in the southern ( $\delta < +2^\circ$ , Meyer et al., 2004) and northern ( $2^\circ < \delta < +25.5^\circ$ , Wong et al. 2005) parts of the survey. The combined HIPASS catalogues cover 29,579 square degrees and the heliocentric velocity range from 300 to 12,700  $\text{km s}^{-1}$ , and contain a total of 5,317 galaxies. HIPASS has a velocity resolution of 18  $\text{km s}^{-1}$  and optical matching shows a  $1\sigma$ -positional accuracy of  $1.4'$  (Doyle et al. 2005), corresponding to less than  $4 h_{100}^{-1}$  kpc at the minimum absorber distance. The HIPASS galaxy catalogue is available at [www.aus-vo.org](http://www.aus-vo.org).

The uniform coverage of HIPASS over such a large fraction of the sky makes it an attractive survey for a cross-correlation function, as no corrections for gaps in the survey are required and edge effects are minimised. A recent study by Cooper et al. (2005) finds that edges and holes in a survey can have a strong effect on measurements of galaxy environment. HIPASS also identifies gas-rich dwarf and low surface brightness galaxies, often missed by magnitude-limited optical surveys. In addition, the dark matter halo masses of HIPASS galaxies have been modelled as a function of HI-mass (Mo et al. 2005), which makes for a straightforward analysis of the bias and clustering properties of HIPASS galaxies.

Random galaxy samples were produced from a Poisson sky distribution with random velocities weighted by the HIPASS selection function (see Figure 1). The random samples each contain  $2 \times 10^4$  sources.

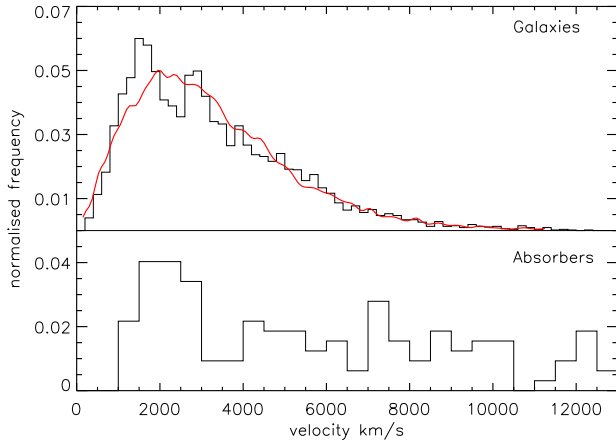


**Figure 1.** Top panel: Velocity histogram of galaxies in the combined HIPASS catalogues, with the HIPASS selection function overdrawn. Bottom panel: Histogram of velocities from the Ly $\alpha$  absorber literature sample.

## 2.2 Ly $\alpha$ absorbers

Low redshift, low column density Ly $\alpha$  absorbers were selected from the Space Telescope Imaging Spectrograph (STIS, Bowen et al. 2002; Penton et al. 2004; Williger et al. 2006) and the Goddard High Resolution Spectrograph (GHRS, Impey et al. 1999; Penton et al. 2000) observations in the literature. These absorbers were chosen to overlap with the combined HIPASS catalogues, i.e.  $\delta < +25^\circ$  and heliocentric velocity between 1,000 and 12,700 km s $^{-1}$ . The lower limit of 1,000 km s $^{-1}$  was applied as many lines-of-sight have significant Galactic absorption features. Only lines with significance level greater than  $4.5\sigma$  were included from Impey et al. (1999) and  $4\sigma$  from Penton et al. (2000), consistent with what these authors considered to be solid detections. The column densities calculated with Doppler parameter  $b = 30$  km s $^{-1}$  are adopted from Penton et al. (2000, 2004). The column densities of the absorbers in the literature sample lie in the range  $12.41 \leq \log(N_{\text{HI}}/\text{cm}^{-2}) \leq 14.81$ , although the 10 absorbers from Impey et al. (1999) only have equivalent width measurements (in the range 0.176 to 1.809 Å). For consistency, each line-of-sight in the sample contains absorbers from a single reference only (the most recent reference is used). There are 129 absorbers from 27 lines-of-sight in the full STIS plus GHRS literature sample.

Although a number of low redshift Ly $\alpha$  absorbers have been detected with the lower resolution Faint Object Spectrograph (FOS, Jannuzi et al. 1998; Bechtold et al. 2002), their equivalent width distribution and velocity uncertainty is quite different from absorbers detected with STIS and GHRS. Furthermore, only 11 additional absorption lines overlap with the HIPASS survey region, thus only absorbers detected with STIS and GHRS have been included in the sample.

Random absorber samples were produced by generating random lines-of-sight on the sky populated with absorbers, where the number distribution of absorbers per random line-of-sight matched the mean (4.8) and standard deviation (3.0) of the absorber sample from the literature. Lines-of-sight with zero absorbers were not included in either the data or random samples. The random absorber velocities are weighted by the velocity distribution of the data absorbers. No evolution is expected or observed in the absorber population over the HIPASS redshift interval  $0 < z < 0.04$  (Penton et al. 2004). The data absorber sample however does not have a flat velocity distribution (see Figure 1). Ideally the absorber

selection function should be constructed from the sum of redshift path lengths of the 27 lines-of-sight, but this information is not available for all lines-of-sight. Most (91/129) of the absorbers in the sample are taken from Penton et al. (2000) or Penton et al. (2004). The path length available for the detection of Ly $\alpha$  absorbers for a superset of these sight-lines (see figure 6 of Penton et al. 2004) is almost a factor of two higher at low redshift ( $z = 0.01$ ) compared with that at the HIPASS redshift limit ( $z = 0.04$ ). This trend is reflected in the shape of the histogram of Ly $\alpha$  absorber velocities in Figure 1. Since the full absorber sample used in this paper is a compilation of data from different observing programs and instruments as well as data reduction, line selection and measurement techniques, weighting the velocity distribution of the random sample will minimise systematic effects of the non-uniform velocity distribution. The final random absorber samples contain around 5,000 absorbers each. Results using the different random absorber samples show no significant variation within the quoted uncertainties.

## 3 CROSS CORRELATION METHOD

The cross-correlation function,  $\xi(\sigma, \pi)$ , is calculated from the Davis & Peebles (1983) estimator,

$$\xi(\sigma, \pi) = \frac{AG(\sigma, \pi) n_{RG}}{RG(\sigma, \pi) n_{AG}} - 1, \quad (1)$$

where  $AG(\sigma, \pi)$  is the number of data absorber–galaxy pairs with projected separation,  $\sigma$ , between  $\sigma - \delta\sigma/2$  and  $\sigma + \delta\sigma/2$ , and radial separation,  $\pi$ , between,  $\pi - \delta\pi/2$  and  $\pi + \delta\pi/2$ .  $RG(\sigma, \pi)$  is the number of pairs consisting of a random absorber and a data galaxy. The projected separation between two objects,  $\sigma_{ij}$ , is converted from angular separation,  $\theta_{ij}$ , by  $\sigma_{ij} = (\text{vel}_i + \text{vel}_j)/H_0 \times \tan(\theta_{ij}/2)$ . The separation along the line-of-sight is simply the velocity difference,  $\pi_{ij} = |\text{vel}_i - \text{vel}_j|/H_0$ . Both  $\delta\sigma$  and  $\delta\pi$  are set at  $0.1 h_{100}^{-1}$  Mpc. The sampling of  $0.1 h_{100}^{-1}$  Mpc is used to ensure a data point exists at reasonably small separations in the correlation function. Equation (1) is calculated in the range 0 to  $100 h_{100}^{-1}$  Mpc in the  $\sigma$  and  $\pi$  directions. The function is normalised by the number of random pairs,  $n_{RG}$ , and data pairs,  $n_{AG}$ . Only pairs with separations less than  $90^\circ$  are included in the calculation (corresponds to  $20 h_{100}^{-1}$  Mpc for the lowest velocity absorbers).<sup>2</sup> The galaxy auto-correlation function is calculated in a similar way, using the random galaxy sample. The spherical average of  $\xi(\sigma, \pi)$  gives the redshift-space correlation function,  $\xi(s)$ , where  $s = \sqrt{\sigma^2 + \pi^2}$ .

The separations used to calculate the cross-correlation function do not take peculiar velocities into account. To reconcile the increased velocity dispersion along the line-of-sight (the finger-of-god effect) the cross-correlation function is integrated along the velocity axis to produce a projected correlation function,  $\Xi(\sigma)$ .

$$\Xi(\sigma) = 2 \int_0^\infty \xi(\sigma, \pi) d\pi \quad (2)$$

In practice the upper limit of the integral is  $50 h_{100}^{-1}$  Mpc, and other upper limits are investigated. The projected and real-space (i.e.  $\xi(r)$ , distortion free) correlation functions are related via

$$\frac{\Xi(\sigma)}{\sigma} = \frac{2}{\sigma} \int_\sigma^\infty \frac{r\xi(r)dr}{\sqrt{r^2 - \sigma^2}} \quad (3)$$

<sup>2</sup> Increasing the maximum separation to  $180^\circ$  produces indistinguishable results for the projected auto- cross-correlations for  $\sigma < 10 h_{100}^{-1}$  Mpc, variations at larger  $\sigma$  are well within the quoted uncertainties.

(Davis & Peebles 1983). If a power law functional form is assumed for the real-space correlation function,  $\xi = (r/r_0)^{-\gamma_r}$ , then the parameters  $r_0$  and  $\gamma_r$  can be derived analytically from the power-law coefficients of the projected correlation function,  $\Xi(\sigma)/\sigma = A(r_0, \gamma_r)\sigma^{-\gamma_r}$ , where

$$A = r_0^{\gamma_r} \Gamma\left(\frac{1}{2}\right) \Gamma\left(\frac{\gamma_r - 1}{2}\right) / \Gamma\left(\frac{\gamma_r}{2}\right) \quad (4)$$

(Davis & Peebles 1983). At large (linear) separations, Mo & White (1996) have used the PS formalism to show that the real-space auto-correlation function of galaxies is related to the dark matter correlation function,  $\xi_{DM}$ , via the bias,  $b$ ,

$$\xi_{gg} = b^2(M_g)\xi_{DM}. \quad (5)$$

This relation has been tested using N-body simulations. An equivalent relation holds for the cross-correlation function of two populations of objects (e.g. Mo et al. 1993), in this case absorbers and galaxies,

$$\xi_{ag} = b(M_a)b(M_g)\xi_{DM}. \quad (6)$$

Thus, the amplitude of cross- to auto- correlation function can be expressed as the ratio of the bias of absorber dark matter haloes,  $b(M_a)$ , to galaxy dark matter haloes,  $b(M_g)$ .

$$\frac{\xi_{ag}}{\xi_{gg}} = \left(\frac{r_{0,ag}}{r_{0,gg}}\right)^{\gamma_{r,gg}} = \frac{b(M_a)}{b(M_g)} \quad (7)$$

As outlined in Mo & White (2002), the ellipsoidal collapse model of bias from Sheth et al. (2001) is more accurate than the original spherical model, hence it shall be adopted here. To directly compare the amplitudes of the cross- and auto-correlation functions, their slopes,  $\gamma_{r,ag}$  and  $\gamma_{r,gg}$ , must be equal. To ensure this the coefficients,  $r_{0,gg}$  and  $\gamma_{r,gg}$ , are calculated first, then  $r_{0,ag}$  is determined by fixing  $\gamma_{r,ag} = \gamma_{r,gg}$  and using a Levenberg-Marquardt non-linear least squares fit. For the auto-correlation function the uncertainties are calculated using jackknife resampling, where the variance,  $\sigma_{\xi}^2$ , is measured by calculating the correlation function  $N$  (24) times, with all data and random points from 1 hour of RA removed each time.

$$\sigma_{\xi}^2 = \frac{N-1}{N} \sum_i (\bar{\xi} - \xi_i)^2 \quad (8)$$

Uncertainties in the cross- and absorber auto- correlation functions are also calculated using jackknife resampling, with one line-of-sight removed each time. Jackknife resampling takes into account cosmic variance within the HIPASS volume and represents the uncertainties more accurately than  $\sqrt{N}$  errors, which are not independent.

In summary, by simply measuring the ratio of the cross- to auto-correlation functions, together with known halo biases and halo masses of galaxies, equation (7) can be used to calculate the mass of haloes in which Ly $\alpha$  absorbers are embedded. This method relies on the assumption that the relative bias can infer a mass for the absorber halo.

## 4 RESULTS

The auto- and cross- correlation functions,  $\xi(\sigma, \pi)_{gg}$  and  $\xi(\sigma, \pi)_{ag}$ , are given in Figures 2 and 3. The finger-of-god effect due to increased velocity dispersion along the line-of-sight is apparent for the galaxy auto-correlation, but is much more exagger-

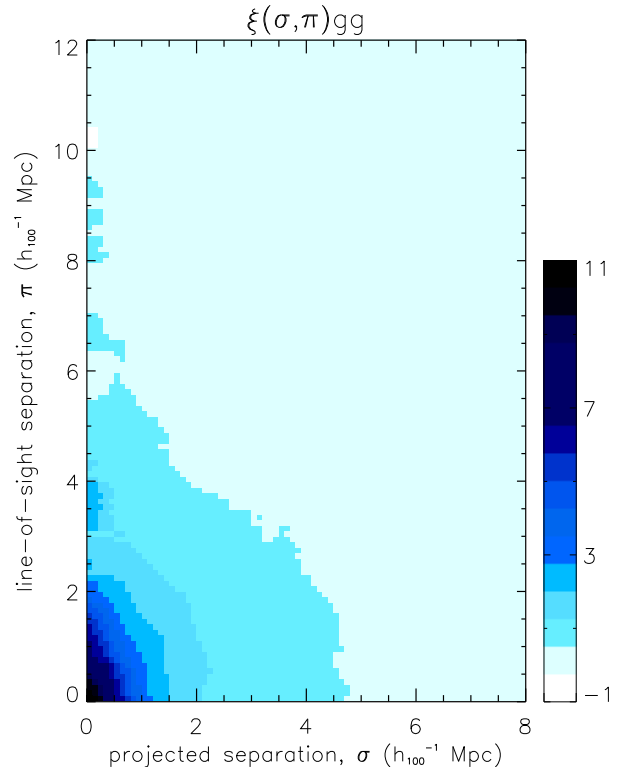


**Figure 2.** The galaxy auto-correlation function. The function is calculated with a resolution of  $\delta\sigma = \delta\pi = 0.1 h_{100}^{-1}$  Mpc and is smoothed with a box-car width of 9 pixels in this diagram. The smoothing level of 9 pixels is used to emphasize features on  $> 1 h_{100}^{-1}$  Mpc scales. Moderate changes to the sampling and smoothing levels do not change these features. Jackknife realisations show typical pixel variations of the order  $\xi_{gg} < 0.2$ .

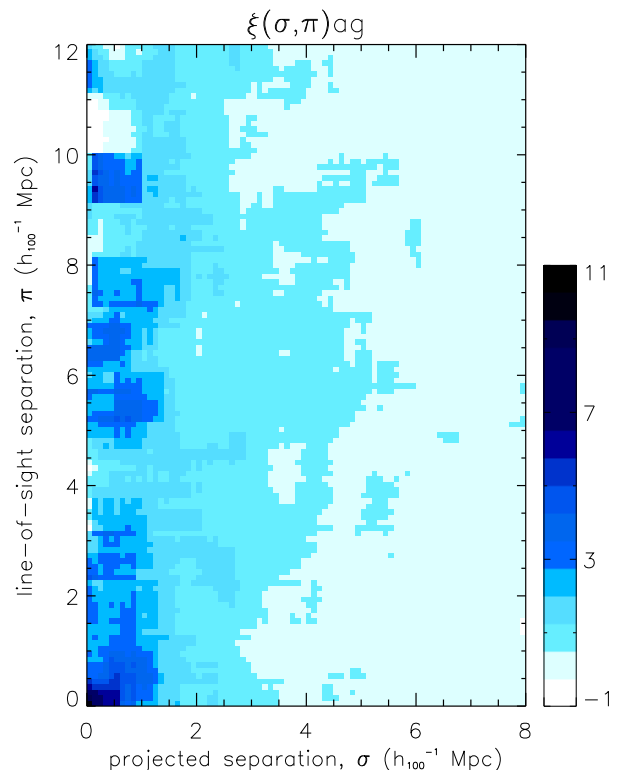


**Figure 3.** The absorber-galaxy cross-correlation function. Smoothing as per Figure 2. Jackknife realisations show typical pixel variations of the order  $\xi_{ag} < 0.5$ .

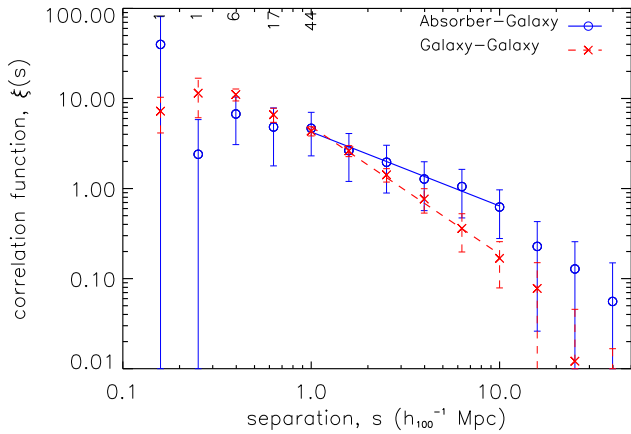


**Figure 4.** The absorber-galaxy cross-correlation function ( $\xi(s)_{ag}$ , circles & solid line) and the galaxy auto-correlation function ( $\xi(s)_{gg}$ , crosses & dashed line) in redshift-space,  $s$ . The five numbers indicate the number of absorber-galaxy pairs that contribute to the first five  $\xi(s)_{ag}$  points in the diagram. See text for power-law fit description. Note that the y-axis range varies from figure to figure.

ated for the absorber-galaxy cross-correlation.<sup>3</sup> The same effect is seen in absorber-galaxy cross-correlation functions from simulations (Davé et al. 1999), and is interpreted as the draining of gas from low-density regions into collapsed structures. Figures 2 and 3 also reveal that at very small separations the auto-correlation signal is stronger, however, the cross-correlation maintains a higher value over a larger section of  $\sigma - \pi$  space. This qualitative comparison suggests that absorbers are not as highly clustered as galaxies on  $< 1 h_{100}^{-1}$  Mpc scales, though not avoiding the highest density regions (which are occupied by galaxies), the normalised chance of finding an absorber at larger scales ( $> 2 h_{100}^{-1}$  Mpc) is more likely than finding another galaxy.

The redshift-space correlation function,  $\xi(s)$ , is calculated from the spherical average of  $\xi(\sigma, \pi)$ . Both the auto- and cross-correlation functions are plotted in Figure 4. Power-law fits to the functions  $\xi(s)_{gg} = (s/s_{0,gg})^{-\gamma_{s,gg}}$  and  $\xi(s)_{ag} = (s/s_{0,ag})^{-\gamma_{s,ag}}$  are made over the range  $1 - 10 h_{100}^{-1}$  Mpc for consistency with the projected correlation function fits (see below). The function parameters are  $s_{0,gg} = 3.1 \pm 0.5 h_{100}^{-1}$  Mpc,  $\gamma_{s,gg} = 1.4 \pm 0.5$ ,  $s_{0,ag} = 6 \pm 4 h_{100}^{-1}$  Mpc, and  $\gamma_{s,ag} = 0.8 \pm 0.2$ . These results can be compared directly with Morris et al. (1993). Their pure Hubble flow galaxy auto-correlation (figure 7a) is marginally higher in amplitude compared with the HIPASS galaxy auto-correlation function. This is expected due to the weaker clustering strength of H I-selected galaxies and is discussed in much detail in Meyer (2003).<sup>4</sup> The absorber-galaxy cross-correlation func-

<sup>3</sup> The elongation along the velocity axis is not dominated by a particular line-of-sight, nor the fact that absorbers are detected along lines-of-sight, nor the absorbers'  $n(z)$ . These possible effects have been investigated by calculating the cross-correlation along each line-of-sight separately, calculating the cross-correlation with one absorber from each line-of-sight only, and considering only absorbers and galaxies with velocities less than  $5,000 \text{ km s}^{-1}$ . In each of these test cases the elongation along the velocity axis remains.

<sup>4</sup> Meyer uses only the southern HIPASS catalogue, the Landy & Szalay (1993) estimator and an integration upper limit of  $25 h_{100}^{-1}$  Mpc, whereas both southern and northern HIPASS catalogues, the Davis & Peebles (1983) estimator and an integration upper limit of  $50 h_{100}^{-1}$  Mpc are use here. The Meyer results lie within the uncertainties quoted here.

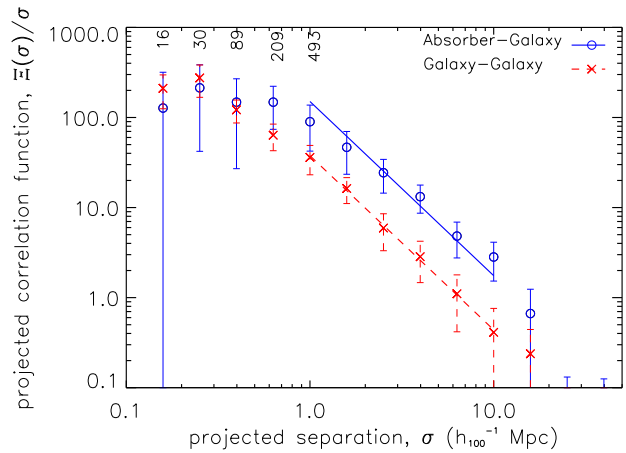


**Figure 5.** The projected absorber-galaxy cross-correlation function (circles & solid line) and the galaxy auto-correlation function (crosses & dashed line). The five numbers indicate the number of absorber-galaxy pairs that contribute to the first five  $\Xi(\sigma)_{ag}$  points in the diagram. See text for power-law fit description.

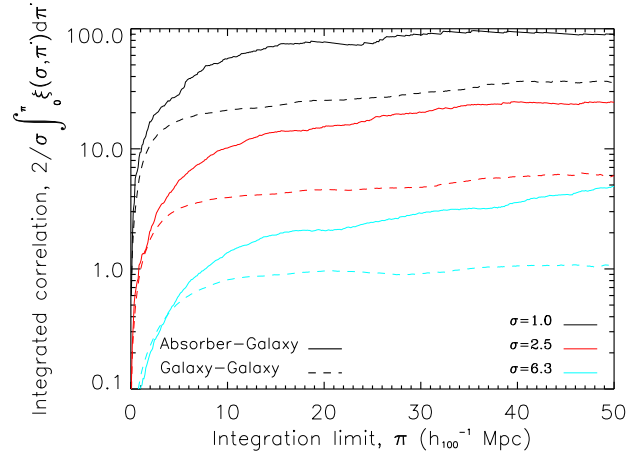


**Figure 6.** Projected cross- and auto-correlation functions compared at different  $\sigma$  values as a function of integration limit,  $\pi$ , see equation (2).

tion of Morris et al. (1993) based on 17 absorbers along the 3C273 line-of-sight is much weaker than the redshift-space correlation presented here, based on 129 absorbers along 27 lines-of-sight. The large uncertainty in the cross-correlation amplitude ( $s_{0,ag} = 6 \pm 4$ ) reflects the large variation from one line-of-sight to another, and emphasises the need for multiple lines-of-sight in this type of analysis.

As described in the method, integrating the correlation function along the velocity axis removes the effect of peculiar velocities along the line-of-sight and allows parameters of the real-space correlation function to be calculated. It is clear from Figure 3 that collapsing  $\xi(\sigma, \pi)$  along the  $\pi$  axis will produce a stronger signal in the absorber-galaxy cross-correlation at projected separations greater than  $1 h_{100}^{-1}$  Mpc. The resulting auto- and cross-correlations are given in Figure 5, and show that the absorber-galaxy cross-correlation is indeed stronger than the HIPASS galaxy auto-correlation for the projected spatial range  $1 - 10 h_{100}^{-1}$  Mpc.

To test the robustness of the projected correlation function, the upper integration limit in Equation (2),  $\pi$ , is varied between 0 and  $50 h_{100}^{-1}$  Mpc. Both the auto- and cross-correlation functions are relatively insensitive to the choice of integration limit. Lowering

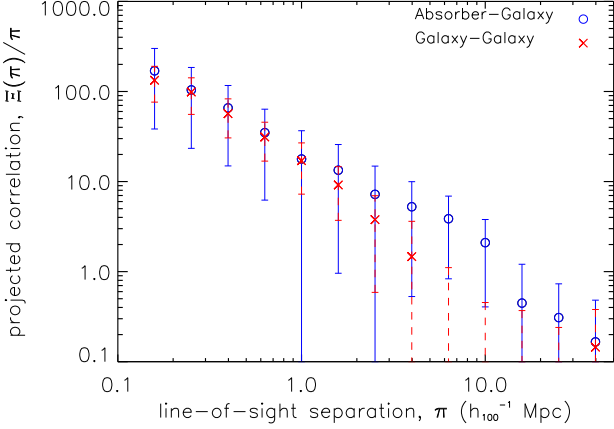


**Figure 7.** The line-of-sight absorber-galaxy cross-correlation function (circles) and the galaxy auto-correlation function (crosses).

the upper limit of the integral does lower the amplitude of both correlation functions slightly, however  $\Xi(\sigma)_{ag}$  remains greater than  $\Xi(\sigma)_{gg}$  over a large area of parameter space. This trend is apparent in Figure 6 where the solid line (cross-correlation) remains above the dashed line (auto-correlation) for displayed values of  $\sigma$  (different shades). Galaxy-galaxy pairs with radial separations greater than  $50 h_{100}^{-1}$  Mpc account for only 6 per cent of the total number of data pairs in the auto-correlation calculation.

Parameters of the projected and real-space correlation functions are calculated by the method described in section 3. The power-law fit is only made over the range  $1 - 10 h_{100}^{-1}$  Mpc since the cross-correlation flattens significantly at small separations and the uncertainties are high at large separations. A correlation length of  $r_{0,gg} = 3.5 \pm 0.7 h_{100}^{-1}$  Mpc and slope of  $\gamma_r = 1.9 \pm 0.3$  is found for the auto-correlation, and  $r_{0,ag} = 7.2 \pm 1.4 h_{100}^{-1}$  Mpc for the cross-correlation. These parameters are plotted on the figure as  $\Xi(\sigma)/\sigma = A(r_0, \gamma_r) \sigma^{-\gamma_r}$  for both the auto- and cross-correlation functions, fixing  $\gamma_{r,ag} = \gamma_r$  for reasons described in the method. Using equation (7) these parameters yield a bias ratio of  $4.0 \pm 1.3$ . The geometric mean HI mass of galaxies contributing to pairs in the range  $1 \leq \sigma \leq 10 h_{100}^{-1}$  Mpc is  $\log(M_{\text{HI}}/M_{\odot}) = 8.8 h_{100}^{-2}$ , with a geometric standard deviation of 1.1. This corresponds to a halo mass of  $\log(M/M_{\odot}) = 11.0 h_{100}^{-1}$  with 1- $\sigma$  lower and upper limits of  $\log(M/M_{\odot}) = 10.8$  and  $11.6$  respectively (Mo et al. 2005). Combining this mean galaxy halo mass, together with the bias ratio calculated above and the linear bias relation (Mo & White 2002) gives a value of  $\log(M/M_{\odot}) = 14.2 h_{100}^{-1}$  (with 1- $\sigma$  lower and upper limits of 13.6 and 14.5 respectively) for the mass of haloes in which Ly $\alpha$  absorbers are embedded. It should be noted that  $\log(M_{\text{HI}}/M_{\odot}) = 8.8 h_{100}^{-2}$  is lower than the geometric mean  $M_{\text{HI}}$  of all HIPASS galaxies because the cross-correlation function is dominated by galaxies located nearby, which on average are lower in HI mass. Nevertheless the bias relation at  $z = 0$  is a relatively flat function of halo mass for halo masses less than  $10^{12} M_{\odot}$ , so the choice of  $M_g$  has little effect on the final result.

The integral of  $\xi(\sigma, \pi)$  along the  $\sigma$  axis is included for comparison with single line-of-sight absorber-galaxy cross-correlation functions that are expressed in terms of velocity separation. An integration limit of  $\sigma = 50 h_{100}^{-1}$  Mpc is used. This function is given in Figure 7, the large error bars reflect the significant variations from one line-of-sight to another in the already weakened correlation signal along the velocity axis due to the finger-of-god effect. As noted in Williger et al. (2006) this calculation produces auto-

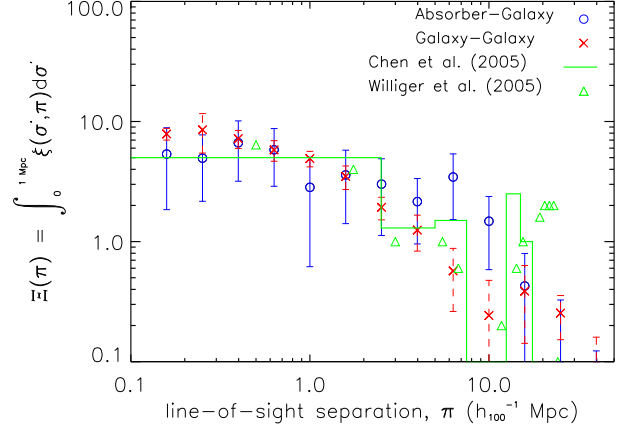


**Figure 8.** The line-of-sight absorber-galaxy cross-correlation function (circles) and the galaxy auto-correlation function (crosses) integrated to  $\sigma = 1 h_{100}^{-1}$  Mpc only to compare with the cylindrical-style cross-correlation functions from Chen et al. (2005) and Williger et al. (2005).

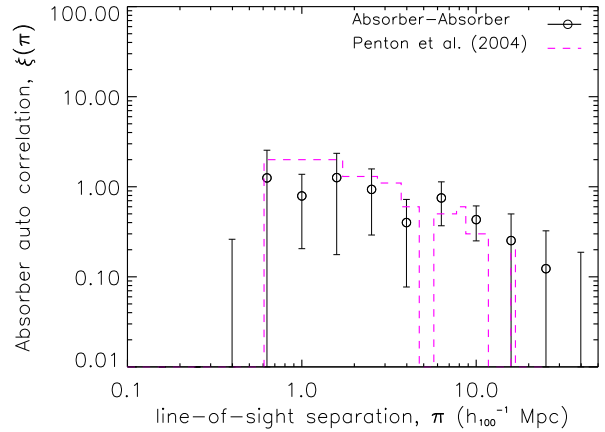


**Figure 9.** Absorber auto-correlation function (circles) with Penton et al. (2004) two-point correlation function,  $\xi(\Delta v)$ , for comparison.

and cross-correlation functions of similar amplitudes. Direct comparisons can be made with the cylindrical-style  $\xi(\Delta v)$  functions of Chen et al. (2005) and Williger et al. (2006) by integrating to  $\sigma = 1 h_{100}^{-1}$  Mpc (although Williger et al. have a projected separation limit that increases from 1 to  $1.6 h_{100}^{-1}$  Mpc along the redshift cylinder) producing the function,

$$\Xi(\pi) = \int_0^{\sigma=1 \text{ Mpc}} \xi(\sigma', \pi) d\sigma', \quad (9)$$

given in Figure 8. Interestingly the cross-correlation drops below the auto-correlation function for  $\sigma < 1 h_{100}^{-1}$  Mpc in agreement with Chen et al. (2005) and Williger et al. (2006), however within the error bars, most points overlap.

Although the mean number of absorbers per line-of-sight is only 4.8, it is still possible to measure the absorber auto-correlation in individual lines-of-sight,

$$\xi(\pi) = \frac{AA(\pi) n_{AR}}{AR(\pi) n_{AA}} - 1, \quad (10)$$

where  $AA(\pi)$  is the number of data absorber pairs with separation,  $\pi$ , and  $AR(\pi)$  is the number of random absorber pairs. Random absorbers are generated as described in Section 2.2. Lines-of-sight

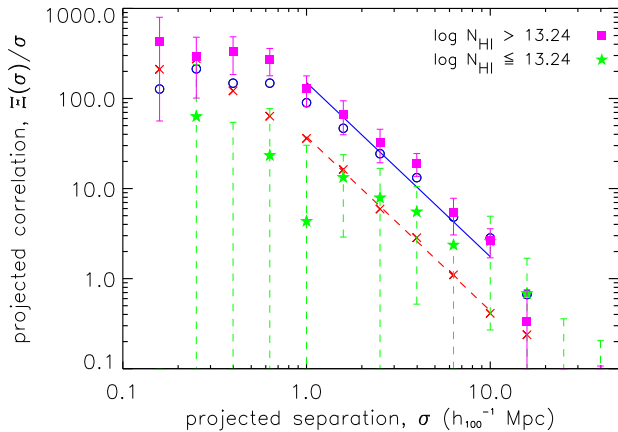


**Figure 10.** The projected absorber-galaxy cross-correlation function for absorbers with  $\log(N_{\text{HI}}/\text{cm}^{-2}) > 13.24$  and  $\log(N_{\text{HI}}/\text{cm}^{-2}) \leq 13.24$ . The cross-correlation from the full absorber data set and galaxy auto-correlation functions from Figure 5 are also plotted for comparison (circles with solid line and crosses with dashed line respectively).

with a single absorber are not included in the calculation. Figure 9 shows that absorbers correlate with themselves very weakly, in agreement with Penton et al. (2004), shown, and also Impey et al. (1999) and Williger et al. (2006). This agreement is anticipated as these absorbers are drawn from those data sets, but still forms a good consistency check as these absorbers represent the first few in each line-of-sight, so there is less opportunity to form pairs.

To test the relationship between absorber column density and correlation strength with galaxies, the absorber sample is split into two subsets defined by the median column density,  $\log(N_{\text{HI}}/\text{cm}^{-2}) = 13.24$ . For consistency with Penton et al. (2002, 2004) a Doppler parameter of  $30 \text{ km s}^{-1}$  is adopted for absorption lines from Impey et al. (1999) to convert the quoted equivalent width measurements into column densities. Random absorber catalogues were re-generated for these sub-samples based on the new velocity distribution, and new mean and standard deviation of each line-of-sight. Figure 10 gives the cross-correlation for absorbers above and below the median  $N_{\text{HI}}$  and shows definite evidence for segregation of lower and higher column density systems. The cross-correlation for absorbers with  $\log(N_{\text{HI}}/\text{cm}^{-2}) > 13.24$  is somewhat stronger than that from the full sample of absorber at projected separations less than  $1 h_{100}^{-1}$  Mpc, although the uncertainties overlap. Low column density absorbers ( $\log(N_{\text{HI}}/\text{cm}^{-2}) \leq 13.24$ ) show a weaker correlation with galaxies, however the uncertainties are large and the results are consistent with no correlation on scales less than  $1 h_{100}^{-1}$  Mpc.

## 5 DISCUSSION

The locations of low- $N_{\text{HI}}$  Ly $\alpha$  absorbers and gas-rich galaxies have been cross-correlated at  $z = 0$ , giving a redshift-space clustering signal similar in strength to that of galaxy self-clustering. The projected cross-correlation removes the increased velocity dispersion along the line-of-sight and from it the real-space clustering can be derived. The cross-correlation function is a powerful statistic as it can be related to the underlying dark matter distribution. Here the absorber cross-correlation results are discussed in relation to mini-haloes, galaxy groups, large-scale filaments, numerical simulations and the environs of gas-rich galaxies.

### 5.1 Ruling out mini-haloes

A typical mini-halo has a circular velocity,  $v_c$ , of  $30 \text{ km s}^{-1}$  (e.g. Mo & Morris 1994), which corresponds to a halo mass and bias of  $6.8 \times 10^9 M_{\odot}$  and 0.73 respectively. Using Equation 7 and the auto-correlation result, such haloes would have a cross-correlation length of  $3.3 h_{100}^{-1}$  Mpc. Comparing this correlation length with the absorber cross-correlation length ( $r_{0,ag} = 7.2 \pm 1.4 h_{100}^{-1}$  Mpc) rules out mini-haloes for the confinement of low- $N_{\text{HI}}$  Ly $\alpha$  absorbers at  $z = 0$  at the 99 percent confidence limit.

### 5.2 Comparison with galaxy groups

The ratio of real-space clustering strengths inferred from the projected correlation functions imply that Ly $\alpha$  absorbers are embedded in haloes with masses in the range  $13.6 < \log(M/M_{\odot}) < 14.5 h_{100}^{-1}$ . This halo mass range is of the same order as the median dynamical mass of galaxy groups in HIPASS,  $\log(M/M_{\odot}) \sim 13.8 h_{100}^{-1}$  (Stevens 2005). This similarity warrants a careful comparison between correlation properties of absorbers and groups.

The cross-correlation between groups and galaxies has been measured with both the Sloan and 2dF galaxy redshift surveys (Yang et al. 2005). The most massive groups (halo mass  $\log(M/M_{\odot}) \leq 13.8 h_{100}^{-1}$ ) display the most elongation along the  $\pi$  axis due to larger velocity dispersions, similar to that seen in the absorber cross-correlation. The shape of the group-galaxy cross-correlation resembles that of the absorber-galaxy cross-correlation at  $\sigma < 2$  and  $\pi < 10$  (Yang et al. 2005, figure 1 – all groups and faintest galaxies), although the group-galaxy correlation level is higher. No 2-D flattening signature of peculiar motions due to infall is seen in the absorber-galaxy cross-correlation, whereas this signature is apparent for groups. The projected correlation is similar in slope at  $1 < \sigma < 10$ , but the flattening of the absorber-galaxy correlation, leads to a much stronger group-galaxy correlation at  $\sigma < 1$ .

The main difference between the correlation properties of absorbers and groups is their self-clustering. Absorber self-clustering (see Figure 9) appears to be weak. The weak clustering could be due to the measurement technique, since absorber self-clustering measurements are restricted to the line-of-sight axis and the clustering signal is elongated, and therefore diluted along this axis. The cross-correlation measured along the redshift axis has almost three times the amplitude as that measured perpendicular to the line-of-sight (compare Figures 5 and 7). Interestingly if the absorber auto-correlation (Figure 9) were increased by a factor of three it would be comparable to the redshift-space galaxy auto-correlation (Figure 4). N-body simulations and analytic models can be used to measure absorber self-clustering in real-space. At least in the case of the warm-hot intergalactic medium (WHIM, slightly higher column densities than the absorbers considered in this paper) the real-space clustering of absorbers at  $r = 1 h_{100}^{-1}$  Mpc could be a factor two less (Valageas et al. 2002) or two more (Davé et al. 2001) than that of galaxies.

Groups of galaxies on the other hand are strongly self-clustered, but not necessarily as strong as their constituent galaxies. More massive haloes are more strongly clustered and contain more galaxies per halo. Thus there are many more galaxies than haloes in strongly clustered environments, and a comparable number of galaxies and haloes in the field. Therefore, purely by relative numbers, galaxies in strongly clustered environments will dominate their correlation function, whereas the correlation signal of groups will be more evenly weighted. This weighting can lead

to the self-clustering signal of groups being *weaker* than that of their constituent galaxies. Naturally, group self-clustering depends on the mass of haloes considered. Padilla et al. (2004) show that the redshift-space correlation length of groups identified in the 2dF galaxy redshift survey increases in amplitude from  $s_0 = 5.5 h_{100}^{-1}$  Mpc for the entire sample, to  $12.6 h_{100}^{-1}$  Mpc for groups with a median mass of  $1.1 \times 10^{14} h_{100}^{-1} M_{\odot}$  (compared with  $s_0 = 6.82 h_{100}^{-1}$  Mpc for 2dF galaxies from Hawkins et al. 2003). The projected auto-correlation of this larger mass group sample is quite similar in amplitude and shape to the Yang et al. (2005) group cross-correlation function described above. Hence it appears that the self-clustering properties of groups are likely to be strong, but could be weaker than galaxies. On the other hand, the self-clustering properties of Ly $\alpha$  absorbers are likely to be weak, but could be as strong as galaxies.

Absorbers, galaxies and groups each trace the underlying dark matter halo distribution in different ways. By comparing the clustering properties of absorbers to that of other objects, the dark matter haloes in which absorber reside can be revealed. As found by many authors (see Section 1), the possibility that Ly $\alpha$  absorbers arise in individual galaxy haloes is unlikely. At a distance of  $20 h_{100}^{-1}$  Mpc, HIPASS is sensitive to galaxies with  $M_{\text{HI}} \geq 2 \times 10^8 h_{100}^{-2} M_{\odot}$ . Considering only galaxies and absorbers within this distance, the nearest galaxy to 50 per cent of absorbers is greater than  $1 h_{100}^{-1}$  Mpc in redshift-space, clearly not within the halo of an individual galaxy. Galaxy groups give a  $\xi(\sigma, \pi)$  diagram that is similar in shape to the absorber-galaxy cross-correlation. In addition, the ratio of real-space clustering lengths imply that Ly $\alpha$  absorbers are embedded in haloes with masses similar to that of galaxy groups. These similarities provide some evidence for the notion that Ly $\alpha$  absorbers are associated with galaxy group environments.

### 5.3 Nature of the correlation signal compared with simulations

Taking the projected absorber-galaxy cross-correlation (Figure 5) at face value, it can be concluded that stepping 1 to  $10 h_{100}^{-1}$  Mpc away from an H I-selected galaxy, the normalised chance of finding an absorber is more likely than finding another galaxy. This likelihood is in addition to the fact that Ly $\alpha$  absorbers are  $\sim 40$  times more frequent than galaxies at zero redshift.<sup>5</sup> The exact covering factor of neutral gas  $1 h_{100}^{-1}$  Mpc away from a galaxy however requires a value for the size of the absorbers, or an assessment of non-detections. At smaller separations the cross-correlation flattens with respect to the galaxy auto-correlation, indicating that at  $< 1 h_{100}^{-1}$  Mpc the normalised chance of encountering a low- $N_{\text{HI}}$  Ly $\alpha$  absorber is less than that of another galaxy - perhaps giving way to higher column density systems. Flattening of the absorber auto-correlation function at a few hundred kiloparsecs is also seen in analytic models and N-body simulations of WHIM absorbers (Davé et al. 2001; Valageas et al. 2002). This length ( $\sim 300$  kpc) corresponds to the characteristic thickness of the WHIM filaments. A fairer comparison can be made with  $\xi(\sigma, \pi)$  diagrams for the cross-correlation of galaxies with low column density absorbers in Davé et al. (1999). Their results suggest the correlation function turns over at small separations, but the interpretation is limited by the resolution of the simulations. The results presented here show

<sup>5</sup> The number density of absorbers with  $13.1 < \log(N_{\text{HI}}/\text{cm}^{-2}) < 14.0$  is  $dN/dz=1.85$  (Penton et al. 2004), the value for gas-rich galaxies is  $dN/dz=0.045$  (Zwaan et al. 2005).

that the cross-correlation flattens at separations less than  $600 h_{100}^{-1}$  kpc. It is possible that this separation corresponds to a characteristic thickness of the large-scale structures in which low column density Ly $\alpha$  absorbers are embedded.

Modelling the low redshift Universe is a complicated business. Ideally the results presented here should be compared with directly with  $\xi(\sigma, \pi)$  and  $\xi(r)$  from simulations and models at zero redshift. Future simulations may be able to distinguish the signature of absorbers embedded in different large-scale structures, for example that of groups or filaments. The essential effect that needs to be tested is whether the elongation along the velocity axis seen in the cross-correlation is due to absorbers that are embedded in a large gravitational potential. Another important insight offered by simulations and models is measuring absorber self-clustering in real-space. Given the large elongation of the absorber-galaxy cross-correlation in redshift-space, and the limitation that absorber self-clustering currently can only be measured along the line-of-sight, it is possible that the self-clustering strength of Ly $\alpha$  absorbers has been understated.

### 5.4 Connection with gas-rich galaxies

Although the HIPASS galaxies are simply used as test particles to represent the underlying density of matter, since they are gas-rich galaxies, gas-rich environments are deliberately selected. Stevens et al. (2004) have shown that the H I content of galaxies in groups detected in HIPASS is no different to field galaxies, in contrast with optically selected groups, which are H I-deficient (Verdes-Montenegro et al. 2001). Thus the intragroup medium of H I-selected groups is expected to have a lower ionization fraction, leading to a higher number of Ly $\alpha$  absorbers. This may explain why Impy et al. (1999) find that absorbers in the vicinity of the Virgo cluster lie preferentially in regions of intermediate (rather than high) galaxy density, since the outskirts of galaxy clusters are known to be in excess of H I-rich galaxies by a factor of three (Waugh et al. 2002). Stocke et al. (2005) find that only 60 per cent of Ly $\alpha$  absorbers with  $\log(N_{\text{HI}}/\text{cm}^{-2}) \gtrsim 13.5$  (corresponding to detected O VI absorption lines) arise in optically selected galaxy groups. Although the difference between optical and H I-selected groups in this case may be due to different sensitivity limits as Stocke et al. (2005) consider galaxy groups with more than one L\* galaxy, whereas HIPASS is sensitive to much fainter galaxies (Doyle et al. 2005).

All galaxies in a representative sample of HIPASS galaxies (Meurer et al. 2005) have been detected in H $\alpha$  emission, and are therefore undergoing star formation. These results emphasize that interstellar hydrogen is a co-requisite for star formation and that HIPASS galaxies can be categorised as emission line galaxies. Interestingly, Chen et al. (2005) finds a stronger Ly $\alpha$  cross-correlation for emission line galaxies, compared with absorption line galaxies, a result that suggests the environs of gas-rich galaxies are preferred by Ly $\alpha$  absorbers.

Despite the large number of absorbers and lines-of-sight, this study is limited by the shallow redshift coverage of HIPASS. Jackknife errors take into account cosmic variance within the HIPASS volume, but not outside the volume. Infrared galaxy counts show that the local area ( $\sim 200 h_{100}^{-1}$  Mpc in linear extent, to a distance of  $\sim 150 h_{100}^{-1}$  Mpc) around the south Galactic pole is underdense by 30 per cent (Frith et al. 2003). Lin et al. (2000) suggest a minimum redshift path length,  $\Delta z$ , of 10 for statistics that discriminate between absorbers arising in galactic haloes and those arising in the cosmic web. The literature sample used in this paper has  $\Delta z \sim 1$

only. HIPASS galaxies also have different clustering properties to optically selected galaxies (Meyer 2003)

For all these reasons it would certainly be worth repeating this study with other galaxy surveys. Future observations designed to measure absorber-galaxy clustering to the same extent as seen here would require a survey of galaxies to projected distances of  $10 h_{100}^{-1}$  Mpc, i.e. for nearby absorbers with velocities around  $10,000 \text{ km s}^{-1}$ , a radius of almost 6 degrees would be required around each quasar, with a depth of at least  $100 h_{100}^{-1}$  Mpc along the line-of-sight.

## 6 SUMMARY

In this paper 129 low column density ( $N_{\text{HI}} < 10^{15} \text{ cm}^{-2}$ ) Ly $\alpha$  absorbers along 27 lines-of-sight have been cross-correlated with 5,317 gas-rich galaxies at  $z = 0$ . A positive association between absorbers and galaxies is found to separations of at least  $10 h_{100}^{-1}$  Mpc in redshift space. The redshift-space auto- and cross-correlation functions are found to be similar in strength, with correlation lengths  $s_{0,gg} = 3.1 \pm 0.5$  and  $s_{0,ag} = 6 \pm 4 h_{100}^{-1}$  Mpc respectively. These results are contrary to that of Morris et al. (1993) based on 17 absorbers along a single line-of-sight, which found a weaker cross-correlation (the uncertainty on  $s_{0,ag}$  is large however, so a weaker correlation for absorbers can only be ruled out at the 53 percent confidence limit). The cross-correlation is found to depend on the column density of the absorbers: higher column density systems ( $\log(N_{\text{HI}}/\text{cm}^{-2}) > 13.24$ ) are more strongly correlated with galaxies, especially at projected separations less than  $1 h_{100}^{-1}$  Mpc.

On a one-to-one basis, out to a distance of  $20 h_{100}^{-1}$  Mpc, 50 per cent of Ly $\alpha$  absorbers are located within  $1 h_{100}^{-1}$  Mpc of a galaxy, and the other half are located  $1 - 3 h_{100}^{-1}$  Mpc from the nearest galaxy. These results agree with many other studies (Bowen et al. 1996, 2002; Tripp et al. 1998; Impey et al. 1999; Penton et al. 2002; Côté et al. 2005) that the majority of Ly $\alpha$  absorbers do not arise in the haloes of individual galaxies. Bearing this result in mind, the cross-correlation function can then be used to measure the extent to which absorbers and galaxies are related.

The amplitude of the absorber-galaxy cross-correlation depends on how it is integrated. The absorber-galaxy  $\xi(\sigma, \pi)$  diagram is very elongated along the line-of-sight. Integrating along the projected separation ( $\sigma$ ) axis produces auto- and cross-correlations with comparable amplitudes. Restricting this integral to  $1 h_{100}^{-1}$  Mpc leads to a cross-correlation that is slightly weaker than the auto-correlation at small separations. Thus results from cylindrical-style cross-correlation functions (Chen et al. 2005; Williger et al. 2006) must be interpreted with caution.

A more conventional approach (as employed in galaxy clustering analysis) is to integrate along the line-of-sight ( $\pi$ ) axis to remove the increased velocity dispersion and from it derive the real-space clustering, and underlying dark matter distribution. The absorber-galaxy cross-correlation has been measured in real-space for the first time here. A correlation length of  $r_{0,ag} = 7.2 \pm 1.4 h_{100}^{-1}$  Mpc is found, compared with  $r_{0,gg} = 3.5 \pm 0.7 h_{100}^{-1}$  Mpc and slope of  $\gamma_r = 1.9 \pm 0.3$  for the galaxy auto-correlation. Mini-halo models on the other hand predict a weaker cross-correlation. The interpretation of these results relies on the assumption that the increased velocity dispersion seen in the cross-correlation is due to a larger gravitational potential. These results rule out mini-halo models for the confinement of low- $N_{\text{HI}}$  Ly $\alpha$  absorbers at  $z = 0$  at the 99 percent confidence limit. The ratio of real-space clustering strengths, together with the bias relation (Equation 7) imply that

Ly $\alpha$  absorbers are embedded in haloes with masses in the range  $13.6 < \log(M/M_{\odot}) < 14.5 h_{100}^{-1}$ , similar to that of galaxy groups. The cross-correlation of massive groups with galaxies produces a  $\xi(\sigma, \pi)$  diagram similar in shape to that of the absorber-galaxy cross-correlation. Thus on average Ly $\alpha$  absorbers tend to follow the same cosmic web of material that embeds both galaxies and groups. This picture is supported by careful analysis of individual systems (Bowen et al. 2002). It is also possible that absorbers arise in filaments of large-scale structure, although the cross-correlation amplitude of filaments has not been measured using observations nor predicted from models or simulations.

The flattening of the cross-correlation function at projected separation less than  $\sim 600 h_{100}^{-1}$  kpc could correspond to a characteristic thickness of the filaments in which Ly $\alpha$  absorber are embedded. A large discrepancy exists between individual Ly $\alpha$  absorber sizes derived from photo-ionization models using metal lines associated with each absorber (10–70 pc, Rigby et al. 2002; Tripp et al. 2002) and their minimum transverse sizes derived from quasar line-of-sight pair analysis (of order  $300 h_{100}^{-1}$  kpc, Penton et al. 2002; Rosenberg et al. 2003). In agreement with Rosenberg et al. (2003), this discrepancy could be reconciled if the minimum transverse size corresponds to the thickness of the filament rather than the individual absorber size. Furthermore, Penton et al. (2002) identify a filament consisting of eight absorbers and five galaxies at least  $20 h_{70}^{-1}$  Mpc across and  $1 h_{70}^{-1}$  Mpc thick. This example fits with the  $\sim 600 h_{100}^{-1}$  kpc filament thickness inferred from the cross-correlation function.

The cross-correlation results presented in this paper provide indirect evidence that Ly $\alpha$  absorbers arise preferentially in gas-rich galaxy groups and filaments. Over half the galaxies in HIPASS occur in groups (Stevens 2005) and gas with  $\log(N_{\text{HI}}/\text{cm}^{-2}) > 13.2$  covers 50 per cent of galaxy filaments (Stocke et al. 2005) – a picture consistent with the ubiquitous nature of Ly $\alpha$  absorbers.

## ACKNOWLEDGMENTS

I wish to acknowledge Lister Staveley-Smith & Rachel Webster who encouraged an early version of this work, Martin Zwaan for providing the HIPASS selection function and Nicolas Bouché for providing  $z = 0$  bias values. This paper would not have been possible without the efforts of the HIPASS team over the last 10 years from survey conception to catalogue completion. I would also like to thank Paul Hewett and Matteo Viel for useful discussions and Nicolas Bouché, Michael Murphy and Max Pettini for comments on the manuscript. The referee, Simon Morris, is also acknowledged for helpful comments that improved the paper. The work in this paper was supported by a PPARC rolling grant at the University of Cambridge.

## REFERENCES

- Adelberger K. L., Shapley A. E., Steidel C. C., Pettini M., Erb D. K., Reddy N. A., 2005, ApJ, 629, 636
- Bechtold J., Dobrzycki A., Wilden B., Morita M., Scott J., Dobrzycka D., Tran K., Aldcroft T. L., 2002, ApJS, 140, 143
- Bouché N., Murphy M. T., Péroux C., 2004, MNRAS, 354, L25
- Bowen D. V., Blades J. C., Pettini M., 1996, ApJ, 464, 141
- Bowen D. V., Pettini M., Blades J. C., 2002, ApJ, 580, 169
- Côté S., Wyse R. F. G., Carignan C., Freeman K. C., Broadhurst T., 2005, ApJ, 618, 178

- Cen R., Phelps S., Miralda-Escude J., Ostriker J. P., 1998, *ApJ*, 496, 577
- Chen H.-W., Lanzetta K. M., Webb J. K., Barcons X., 1998, *ApJ*, 498, 77
- Chen H.-W., Lanzetta K. M., Webb J. K., Barcons X., 2001, *ApJ*, 559, 654
- Chen H.-W., Prochaska J. X., Weiner B. J., Mulchaey J. S., Williger G. M., 2005, *ApJ*, 629, L25
- Cole, S. et al 2001, *MNRAS*, 326, 255
- Cooper M. C., Newman J. A., Madgwick D. S., Gerke B. F., Yan R., Davis M., 2005, *ApJ*, 634, 833
- Davé R., Cen R., Ostriker J. P., Bryan G. L., Hernquist L., Katz N., Weinberg D. H., Norman M. L., O'Shea B., 2001, *ApJ*, 552, 473
- Davé R., Hernquist L., Katz N., Weinberg D. H., 1999, *ApJ*, 511, 521
- Davé R., Katz N., Weinberg D. H., 2003, in *ASSL Vol. 281: The IGM/Galaxy Connection. The Distribution of Baryons at z=0*, *ASSL Conference Proceedings Vol. 281*. Edited by Jessica L. Rosenberg and Mary E. Putman. Kluwer Academic Publishers, Dordrecht p. 271
- Davis M., Peebles P. J. E., 1983, *ApJ*, 267, 465
- Dobrzycki A., Bechtold J., Scott J., Morita M., 2002, *ApJ*, 571, 654
- Doyle, M. T. et al 2005, *MNRAS*, 361, 34
- Frith W. J., Busswell G. S., Fong R., Metcalfe N., Shanks T., 2003, *MNRAS*, 345, 1049
- Grogin N. A., Geller M. J., 1998, *ApJ*, 505, 506
- Hawkins, E. et al 2003, *MNRAS*, 346, 78
- Ikeuchi S., 1986, *Ap&SS*, 118, 509
- Impey C. D., Petry C. E., Flint K. P., 1999, *ApJ*, 524, 536
- Jannuzi B. T., Bahcall J. N., Bergeron J., Bokserberg A., Hartig G. F., Kirhakos S., Sargent W. L. W., Savage B. D., Schneider D. P., Turnshek D. A., Weymann R. J., Wolfe A. M., 1998, *ApJS*, 118, 1
- Landy S. D., Szalay A. S., 1993, *ApJ*, 412, 64
- Lanzetta K. M., Bowen D. V., Tytler D., Webb J. K., 1995, *ApJ*, 442, 538
- Lanzetta K. M., Webb J. K., Barcons X., 1996, *ApJ*, 456, L17
- Le Brun V., Bergeron J., Boisse P., 1996, *A&A*, 306, 691
- Lin W. P., Börner G., Mo H. J., 2000, *MNRAS*, 319, 517
- Liske J., Webb J. K., Williger G. M., Fernández-Soto A., Carswell R. F., 2000, *MNRAS*, 311, 657
- Madau P., Ferrara A., Rees M. J., 2001, *ApJ*, 555, 92
- McDonald P., Miralda-Escudé J., Cen R., 2002, *ApJ*, 580, 42
- McLin K. M., Stocke J. T., Weymann R. J., Penton S. V., Shull J. M., 2002, *ApJ*, 574, L115
- Meurer, G. R. et al. 2005, *ApJS*, submitted
- Meyer M. J., 2003, Ph.D. Thesis, U. Melbourne
- Meyer M. J., et al. 2004, *MNRAS*, 350, 1195
- Mo H. J., Morris S. L., 1994, *MNRAS*, 269, 52
- Mo H. J., Peacock J. A., Xia X. Y., 1993, *MNRAS*, 260, 121
- Mo H. J., White S. D. M., 1996, *MNRAS*, 282, 347
- Mo H. J., White S. D. M., 2002, *MNRAS*, 336, 112
- Mo H. J., Yang X., van den Bosch F. C., Katz N., 2005, *MNRAS*, 363, 1155
- Morris S. L., Weymann R. J., Dressler A., McCarthy P. J., Smith B. A., Terrile R. J., Giovanelli R., Irwin M., 1993, *ApJ*, 419, 524
- Ortiz-Gil A., Lanzetta K. M., Webb J. K., Barcons X., Fernández-Soto A., 1999, *ApJ*, 523, 72
- Padilla, N. D. et al 2004, *MNRAS*, 352, 211
- Penton S. V., Shull J. M., Stocke J. T., 2000, *ApJ*, 544, 150
- Penton S. V., Stocke J. T., Shull J. M., 2002, *ApJ*, 565, 720
- Penton S. V., Stocke J. T., Shull J. M., 2004, *ApJS*, 152, 29
- Porciani C., Madau P., 2005, *ApJ*, 625, L43
- Press W. H., Schechter P., 1974, *ApJ*, 187, 425
- Putman M. E., Rosenberg J. L., Stocke J. T., McEntaffer R., 2006, 131, 771
- Rao S. M., Turnshek D. A., Nestor D. B., 2006, *ApJ*, 636, 610
- Rees M. J., 1986, *MNRAS*, 218, 25
- Rigby J. R., Charlton J. C., Churchill C. W., 2002, *ApJ*, 565, 743
- Rosenberg J. L., Ganguly R., Giroux M. L., Stocke J. T., 2003, *ApJ*, 591, 677
- Sheth R. K., Mo H. J., Tormen G., 2001, *MNRAS*, 323, 1
- Stevens J. B., 2005, Ph.D. Thesis, U. Melbourne
- Stevens J. B., Webster R. L., Barnes D. G., Pisano D. J., Drinkwater M. J., 2004, *Publications of the Astronomical Society of Australia*, 21, 318
- Stocke J. T., Penton S. V., Danforth C. W., Shull J. M., Tumlinson J., McLin K. M., 2005, *ApJ*, submitted, astro-ph/0509822
- Tripp T. M., Jenkins E. B., Williger G. M., Heap S. R., Bowers C. W., Danks A. C., Davé R., Green R. F., Gull T. R., Joseph C. L., Kaiser M. E., Lindler D., Weymann R. J., Woodgate B. E., 2002, *ApJ*, 575, 697
- Tripp T. M., Lu L., Savage B. D., 1998, *ApJ*, 508, 200
- Ulmer A., 1996, *ApJ*, 473, 110
- Valageas P., Schaeffer R., Silk J., 2002, *A&A*, 388, 741
- Verdes-Montenegro L., Yun M. S., Williams B. A., Huchtmeier W. K., Del Olmo A., Perea J., 2001, *A&A*, 377, 812
- Waugh, M. et al. 2002, *MNRAS*, 337, 641
- Williger G. M., Heap S. R., Weymann R. J., Davé R., Ellingson E., Carswell R. F., Tripp T. M., Jenkins E. B., 2006, *ApJ*, 636, 631
- Wong, O. I. et al. 2005, *MNRAS*, submitted
- Yang X., Mo H. J., van den Bosch F. C., Weinmann S. M., Li C., Jing Y. P., 2005, *MNRAS*, 362, 711
- Zwaan M. A., van der Hulst J. M., Briggs F. H., Verheijen M. A. W., Ryan-Weber E. V., 2005, *MNRAS*, 364, 1467
- Zwaan, M. A. et al. 2003, *AJ*, 125, 2842

This paper has been typeset from a  $\text{\TeX}/\text{\LaTeX}$  file prepared by the author.